Phenyl Ring Dynamics in a Tetraphenylethylene-Bridged Metal–Organic Framework: Implications for the Mechanism of Aggregation-Induced Emission

Citation: Shustova, Natalia B., Ta-Chung Ong, Anthony F. Cozzolino, Vladimir K. Michaelis, Robert G. Griffin, and Mircea Dincă. "Phenyl Ring Dynamics in a Tetraphenylethylene-Bridged Metal–Organic Framework: Implications for the Mechanism of Aggregation-Induced Emission." Journal of the American Chemical Society 134, no. 36 (September 12, 2012): 15061-15070.

As Published: http://dx.doi.org/10.1021/ja306042w

Publisher: American Chemical Society (ACS)

Persistent URL: http://hdl.handle.net/1721.1/82041

Version: Author's final manuscript: final author's manuscript post peer review, without publisher's formatting or copy editing

Published in final edited form as:
J Am Chem Soc. 2012 September 12; 134(36): 15061–15070. doi:10.1021/ja306042w.

Phenyl Ring Dynamics in a Tetraphenylethylene-Bridged Metal-Organic Framework: Implications for the Mechanism of Aggregation-Induced Emission

Natalia B. Shustova[†], **Ta-Chung Ong**[†,‡], **Anthony F. Cozzolino**[†], **Vladimir K. Michaelis**[†,‡], **Robert G. Griffin**[†,‡,*], and **Mircea Dincă**[†,*]

[†]Department of Chemistry, Massachusetts Institute of Technology, Cambridge, Massachusetts, USA, 02139

[‡]Francis Bitter Magnet Laboratory, Massachusetts Institute of Technology, Cambridge, Massachusetts, USA, 02139

Abstract

Molecules that exhibit emission in the solid state, especially those known as aggregation-induced emission (AIE) chromophores, have found applications in areas as varied as light-emitting diodes and biological sensors. Despite numerous studies, the mechanism of fluorescence quenching in AIE chromophores is still not completely understood. To this end, much interest has focused on understanding the low frequency vibrational dynamics of prototypical systems such as tetraphenylethylene (TPE), in the hope that such studies would provide more general principles towards the design of new sensors and electronic materials. We hereby show that a perdeuterated TPE-based metal-organic framework (MOF) serves as an excellent platform for studying the low energy vibrational modes of AIE-type chromophores. In particular, we use solid-state ^{2}H and ^{13}C NMR experiments to investigate the phenyl ring dynamics of TPE cores that are coordinatively trapped inside a MOF and find a phenyl ring flipping energy barrier of 43(6) kJ/mol. DFT calculations are then used to deconvolute the electronic and steric contributions to this flipping barrier. Finally, we couple the NMR and DFT studies with variable temperature X-ray diffraction experiments to propose that both the ethylenic C=C bond twist and the torsion of the phenyl rings are important for quenching emission in TPE, but that the former may gate the latter. To conclude, we use these findings to propose a set of design criteria for the development of tunable turn-on porous sensors constructed from AIE-type molecules, particularly as applied to the design of new multifunctional MOFs.

Introduction

The relaxation of singlet excited states in light-absorbing molecules occurs either by emission of a photon, giving rise to fluorescence, or non-adiabatically, through non-radiative decay pathways.[1] In most cases, chromophores that show high fluorescence quantum yields in dilute solutions become non-fluorescent in colloids and in the solid-state, where intermolecular interactions such as π-stacking often cause self-quenching.[2] This effect, sometimes referred to as aggregation-caused quenching, poses significant difficulties for the development of solid-state fluorescence devices such as organic light-emitting diodes and luminescence-based sensors.[2–4] A diametrically-opposed effect is operative, however, in a

Corresponding Author: mdinca@mit.edu, rgg@mit.edu.

Supported Information. X-ray structure refinement tables and details, NMR spectra, TGA traces, DFT-calculated molecular conformations and PESs, and emission spectra. This material is available free of charge via the Internet at http://pubs.acs.org.

select class of chromophores that exhibit weak or almost no fluorescence in dilute solutions, but show high fluorescence quantum yields in colloidal aggregates and in the solid state.[5,6] This opposite effect, known as aggregation-induced emission (AIE), is observed in molecules that contain groups executing fast discrete diffusion, such as twofold or threefold hops by phenyl or trimethylsilyl rotors, respectively. These moieties are bonded to relatively inflexible backbones such as ethylenic C=C bonds or rigid rings such as silole.[7–9] The discovery of the AIE effect and its wide potential for applicability in biological and environmental sensors,[10–14] solid-state lighting devices,[4,6,15] and luminescent polymers[16,17] has sparked a rapid expansion of the field in the past decade. Despite these advancements, the exact mechanism of AIE continues to be a subject of interest for theoreticians and experimentalists alike; deciphering it unequivocally would clearly be beneficial for the *ab-initio* development of new classes of AIE molecules.[18,19] Generally, AIE arises because rotor-containing molecules exhibit low frequency vibrational modes in the gas phase or in dilute solutions. These modes are responsible for very fast non-radiative decay of the singlet excited state but are eliminated in the solid state due to intermolecular steric interactions. For instance, tetraphenylethylene (TPE), one of the most accessible and simplest AIE-type chromophores, exhibits low-frequency phenyl torsion modes and C=C twist modes (Figure 1) that are deactivated in the solid state by close intermolecular arene···H and Ph···Ph interactions.[5,19,20] Understanding the relative contribution and effect of these vibrational modes and conformational changes is one of the keys to making more efficient and more sensitive fluorescence turn-on sensors from rotor-containing chromophores.

To this end, we sought to understand the mechanism that induces fluorescence in a TPE-based metal-organic framework (MOF) reported recently by us.[21] Although the formation of close intermolecular contacts had previously been presumed necessary for turning on emission in rotor-containing chromo-phores,[5] we showed that coordination of phenyl groups to metal atoms within MOFs also turns on the fluorescence of the TPE cores. One such material, Zn_2(TCPE)(solvent)$_2$ (**1H**; TCPE = tetrakis(4-carboxyphenyl)ethylene), exhibits arene···H and Ph···Ph interactions on neighboring TPE cores that are 1.5 Å longer than in molecular TPE aggregates (Figure 1).[21] Although these distances are sufficient to allow unimpeded rotation/flipping of the phenyl rings,[22] **1H** is fluorescent. We surmised that because the carboxylate groups in H_4TCPE are installed in the para position, phenyl ring flipping and/or libration in **1H** is not completely eliminated, and that understanding the mechanism of fluorescence turn-on in **1H** would therefore aid in the design of efficient emitters and more sensitive, guest-induced turn-on fluorescence sensors. Our interest in studying the dynamics of phenyl ring motion in TPE-based MOFs was therefore motivated by the possibility of providing general principles towards the formation of high-surface area turn-on fluorescent sensors from AIE-type chromophores. In doing so, we were also hoping to shed more light on the mechanism of aggregation-induced emission and thereby provide guidance for the development of new chromophores in this rapidly expanding area.

With these goals in mind, we synthesized a deuterated TPE-based MOF that is structurally analogous to **1H** and employed ^{2}H NMR spectroscopy and ^{13}C cross-polarized magic angle spinning solid-state (CP MAS) NMR spectroscopy to determine the activation barrier for phenyl ring flipping in this material. In conjunction with temperature-dependent single-crystal and powder X-ray diffraction analysis and density functional theoretical calculations, these results reveal that fluorescence is turned-on in TPE-based MOFs by *drawing* of the TPE core rather than the presence of close intermolecular Ph···Ph interactions, as is typical for molecular constructs of rotor-containing chromophores. Accordingly, we propose that both the C=C bond twist and the torsion of the phenyl rings are important for quenching emission in TPE, but that the former may gate the latter. We use these findings to propose a set of design criteria for the development of tunable turn-on porous sensors constructed from AIE-type molecules.

Results

Synthesis and temperature-dependent structural studies

Synthesis of a deuterated TPE-based MOF started from deu-tero-tetra(4-carboxy)phenylethylene, H_4TCPE-d_{16}, which was accessed from perdeuterated benzene in four steps, shown in Scheme 1. Treatment of C_6D_6 with oxalyl chloride in carbon disulfide produced benzophenone-d_{10}, which was subsequently homocoupled under McMurry condensation conditions[23] to yield TPE-d_{20}. Bromination of TPE-d_{20} with neat Br_2 followed by copper-catalyzed halide-for-cyanide exchange and basic hydrolysis of the nitrile groups gave the desired tetracarbox-ylate ligand, H_4TCPE-d_{16} in 31% overall yield. Heating a solution of H_4TCPE-d_{16} and $Zn(NO_3)_2{\cdot}6H_2O$ in a mixture of ethanol and *N*,*N*-diethylformamide (DEF) at 75 °C for three days produced yellow block-shaped crystals of Zn_2(TCPE- d_{16})$(DEF)_2{\cdot}2$DEF (**1a**).

An X-ray diffraction study of a single crystal of **1a** revealed a structure in which $Zn_2(O_2C\text{-})_4$ paddlewheel units are bridged by $TCPE^{4-}$-d_{16} ligands in infinite two-dimensional sheets whose connectivity is identical to that found in **1H**.[21] The sheets adopt a staggered conformation to give similar, but not identical lattice parameters to those of **1H**, as shown in Table S1. Despite the slight shift in the stacking arrangement of the 2D sheets in **1a** relative to **1H**, the two related structures exhibit almost identical fluorescence spectra and thermal behavior, evidenced in the thermogravimetric analysis traces shown in Figure S1. As in **1H**, thermal treatment of **1a** produces several significant structural transformations. Since these are crucial for the interpretation of the NMR data, we undertook variable temperature X-ray diffraction studies of both TPE-d_{20} and **1**. Thus, the X-ray crystal structure of TPE-d_{20} was determined at 93 K, 298 K, and 373 K. TPE-d_{20} maintains the monoclinic $P2_1$ space group at all three temperatures, with no significant changes in lattice parameters, molecular packing, or Ph···Ph ring intermolecular distance. As shown in Table S2, the shortest inter-chromophore contacts (Ph···Ph ring contacts) are 3.583(3)–3.635(5) Å, while the twist of the C=C bond (Figure 1) is 8.84–10.16°. Over the entire temperature range, the shortest intermolecular TPE contacts change by no more than 0.052(6) Å, and the change in the C=C twist angle is less than 1.32°. Single crystal X-ray structures of **1** were also determined at 100 K and 373 K. As shown in Figure 2, 1 adopts a monoclinic structure at 100 K (**1a**), but undergoes a symmetry-increasing transformation to an orthorhombic phase while heating to 373 K, which we designate as **1b**. Importantly, powder X-ray diffraction analysis revealed that the 2D sheets do not change their relative positioning upon transformation from **1a** to **1b**. Determination of the unit cell parameters of **1a** at room temperature confirmed only very small deviations from the orthorhombic cell determined at 373 K for **1b**. Apart from the small deviation in overall symmetry, important structural differences between the structures of **1a** and **1b** include the lack of guest DEF molecules in the latter, an extension of the shortest Ph···Ph contacts from 4.744(9) to 5.10(1) Å and a reduction of the ethylene twist angle from 5.35° to 3.83°. The lack of guest DEF molecules in **1b**, formulated as Zn_2(TCPE-d_{16})$(DEF)_2$, is in agreement with the thermogravimetric analysis (TGA) and elemental analysis data (vide infra).

Continued heating at 200 °C caused a complete loss of Zn-coordinated DEF molecules. PXRD analysis revealed that this is also accompanied by a drastic structural rearrangement to a desolvated form of **1**, Zn_2(TCPE-d_{16}) (**1c**). Because single crystals of **1b** do not survive their transformation into **1c**, we sought to match the observed PXRD pattern of **1c** with a structural model. This was accomplished by implementing an original computational routine in Matlab®, which simulate PXRD patterns of possible phases by changing the interlayer distance and relative displacement of 2D layers. In this case, the structure of **1b** was used as an initial model, and we considered the possibility that **1c** is related to the former by simple

translations of the 2D sheets in the *ab* plane and/or by changes in the inter-sheet separation. Modulation of these parameters using our routine provided a structural model for **1c** that exhibited a good match with the observed pattern (Figure S2). Although the relatively poor crystallinity of **1c** prevented a full Rietveld refinement even from synchrotron-collected data, our computational routine revealed that **1c** is a new orthorhombic phase with parameters of 12.66, 8.40, and 21.62 Å.

The one notable difference between **1b** and **1c** is the much reduced interlayer distance, which decreases from 8.7 Å in the former to 4.2 Å in the latter (Figure 2). The contraction of the interlayer distance brings the $Zn_2(O_2C\text{-})_4$ paddlewheel units in neighboring 2D sheets in close proximity and prompts the formation of covalent linkages between Zn atoms in one sheet and carboxylate oxygen atoms in adjacent sheets. The absence of all DEF molecules from **1c** was confirmed by thermogravi-metric analysis, which showed a mass loss of 36.2 % below 200 °C, in agreement with the 35.4% expected for the elimination of four DEF molecules from **1a** (Figure S1).

^{1}H, ^{13}C, and ^{2}H NMR Spectroscopic Studies

Variable temperature ^{1}H NMR spectra of TPE and H_4TCPE were rec- orded in CD_2Cl_2 and CD_3OD, respectively, between 183 K and 293 K. The phenyl ring protons appear as a pair of doublets with chemical shifts of 7.14 and 7.81 ppm ($^{3}J_{HH}$ = 8 Hz) for H_4TCPE, and two multiplets with shifts at 7.03 and 7.10 ppm for TPE itself. As shown in Figure S3, cooling to 183 K broadens the ^{1}H resonances in both TPE and H_4TCPE, but the two different proton signals do not coalesce, suggesting that the phenyl rings in both molecules are in the fast exchange regime in solution even at 183 K. To confirm the expected slow exchange regime of phenyl rings in TPE-d_{20} in the solid state, ^{2}H NMR spectra of crystalline samples of this molecule were recorded between 298 and 423 K. As shown in Figure S4, the ^{2}H NMR spectra of solid TPE-d_{20} in this temperature range exhibit two peaks separated by Q = 128 kHz. This yields a Pake pattern characteristic of C-^{2}H vectors in the slow exchange regime ($\tau > 10^{-3}$–10^{-4} s).[24] ^{2}H quadrupolar echo spectroscopy was also used to investigate the phenyl ring dynamics in **1a** and **1c**. As shown in Figure S5, **1c** showed almost identical Pake patterns up to 423 K, the highest temperature achievable with our NMR probe. In contrast, freshly synthesized **1a** showed Pake patterns only between room temperature and approximately 323 K. Heating **1a** above 323 K caused the line shape to evolve into a pattern wherein a second set of symmetric peaks with a smaller splitting of Q/4 = 32 kHz emerged along with a third wider splitting being −5Q/−4 = 160 kHz. As shown in Figure 3, the intensity of this central set gradually increased at the expense of the original outer signal up to 423 K. An isotropic signal also became apparent above 323 K, likely indicative of the increased mobility of the guest DEF molecules. Indeed, this isotropic signal disappeared after prolonged heating at 423 K, indicating the loss of the guest molecules and conversion to **1b**. Upon cooling of **1b**, the reverse evolution of the quadrupolar signal was observed; the twofold flip pattern at 423 K gradually evolved into a typical slow-exchange Pake pattern at 323 K.

To simulate the spectra we assumed a model consisting of a single population of phenyl rings undergoing discrete two-fold flips. The model was used for simulations of the ^{2}H quadrupo-lar line shapes for five temperatures during the cooling cycle of **1b** between 421 K and 321 K.[25,26] The simulations yielded flipping rates of 1.2×10^{6}, 2.0×10^{5}, 3.2×10^{4}, 1.8×10^{4}, and 1.0×10^{4} Hz at 421, 369, 345, 321, and 300 K, respectively. To obtain an activation energy and pre-exponential factor for phenyl ring flipping in **1b**, the natural logarithm of the rates was plotted against the inverse of the respective temperatures to give an Arrhenius plot. A line fit to this graph, shown in Figure 4, gave activation energy and pre-exponential factor values of 43(6) kJ/mol and 2.2×10^{11} Hz, respectively. Although ^{2}H

NMR revealed a wealth of information about the phenyl ring dynamics in **1b**, it was not suitable to interrogate the same in **1c**, where the phenyl ring motion remains in the slow regime ($<10^4$ Hz) regardless of the temperature (*vide supra*). Because ^{13}C CP MAS NMR spectroscopy can be used to probe motions down to frequencies of ~10^2 Hz,[27] ^{13}C CP MAS-NMR spectra were acquired for **1c** and its protonated relative (fully desolv-ated **1H**) at room temperature. As shown in Figure 5, both deuterated and protonated versions of the MOFs exhibit isotropic peaks at 135, 137 and 153 ppm for the phenyl ring carbon atoms, and 147 and 181 ppm for the ethylene and carboxylate carbon atoms, respectively.

Theoretical Studies

DFT was employed to calculate the activation barrier for ring flipping in **1b**. The barrier was estimated by modeling the potential energy surface (PES) of $TCPE^{4-}$ bound by four $Zn_2(O_2C–)_4$ paddlewheels. The metal coordination sphere was completed with three bridging formate ligands and two terminal water ligands (Figure 6).

The PES was constructed by varying one $C_{Ar}–C_{Ar}–C=C$ dihedral angle from 0 to 180° and is depicted in Figure 7.. The Zn and oxygen atom coordinates were fixed in order to mimic the rigidity imposed by the framework. Notably, a very similar PES could be obtained using H_4TCPE with the oxygen atom coordinates fixed to those found in the **1** (Figure S7) with significant savings in computational resources. The lowest energy structure structure from the PES, which was deemed closest to the absolute minimum energy conformation, was used as a starting point for a geometry optimization to find the absolute minimum. Because of the size of the system under investigation, a transition state was not modeled. Under these parameters, the activation energy for a ring flip in **1b** was estimated at 49 kJ/mol.

The DFT-estimated activation barrier for phenyl ring-flipping in TPE in the gas phase is 24 kJ/mol. This value was determined by first modeling the PES by varying the $C_{Ar}–C_{Ar}–C=C$ dihedral angle from 0 to 180° and 180 to 0° with no additional constraints (Figure 8). To correct for false maxima that could arise due to the high number of degrees of freedom, a minimum energy PES was constructed by convoluting PESs calculated in the forward and reverse directions of phenyl ring rotation.

As before, the lowest energy structure on the convoluted PES was used as a starting point for a geometry optimization and was confirmed by a frequency calculation that provided no negative values. Notably, we calculated a barrier of 49 kJ/mole for the truncated model of **1b** in the vicinity of 0°, a value that is approximately 25 kJ/mol higher in energy than that calculated for TPE at the same angle. The structure of TPE at the maxima reveals an ethylene core that has undergone significant structural deviation from the minimum energy structure in- volving the $C_{Ar}–C=C–C_{Ar}$ and $C_{Ar}–C_{Ar}–C=C$ dihedral angles as well as the $C_{Ar}–C_{(ethylene)}–C_{Ar}$ and $C_{Ar}–C=C$ bond angles (Figure 6), whereas the constraints imposed by the rigid framework in **1b** prevent the ethylene core from undergoing similar distortions (Tables S3–S6). The structural distortions in TPE correspond to the lowest energy vibrational modes (Table 1) that occur well below kT (206 cm^{-1} at 298 K).

In order to deconvolute the steric from the electronic effects in the barriers in the PESs for the truncated model of **1b** and for TPE, PESs for the ring flipping of the phenyl ring in styrene and benzoic acid were constructed under the assumption that the PESs for these two systems provide a rotational barrier that is free of steric effects. In both cases, the minimum in energy occurs when the $C_{Ar}–C_{Ar}–C=C$ dihedral angle is 0°, which corresponds to the geometry that maximizes the conjugation between the phenyl ring and the pendant group (Figure S6). The associated calculated activation energies for phenyl ring flipping in styrene and benzoic acid are 18 kJ/mol and 27 kJ/mol, respectively.

Discussion

The structure of **1a** consists of a two-dimensional frame- work composed of paddlewheel $Zn_2(O_2C\text{-})_4$ secondary building units that are bridged by $TCPE^{4-}$-d_{16} ligands (Figures 1 and 2). The structure contains both bound DEF molecules, which occupy the axial sites on Zn atoms in the Zn_2 paddlewheels, and guest DEF molecules, which occupy the pores. The latter likely prevent fast flipping of the TPE phenyl rings, and ^{2}H NMR spectra of **1a** accordingly reveal Pake patterns characteristic of slow-exchange (< 10^4 Hz). The Pake patterns persist up to 373 K, but heating **1a** above this temperature starts liberating the guest DEF molecules, thereby activating the phenyl ring flips. Indeed, ^{2}H NMR spectra at 373 K, 396 K, and 423 K reveal an isotropic signal that can be attributed to solvent motion, and dynamic quadrupole patterns that can be fit to discrete 180° phenyl ring flips with respective frequencies shown in Figure 3. Because both guest solvent loss and activation of phenyl ring dynamics take place during heating of **1a**, the two processes are convoluted and prevent an Arrhenius analysis. Instead, the sample was kept at 423 K for 24 hours to eliminate all of the guest solvent molecules and complete conversion of **1a** into **1b**, as identified by the disappearance of the isotropic signal attributed to mobile DEF. ^{2}H NMR data was again collected for **1b** on cooling back to room temperature, with data points at 421, 369, 345, 321, and 300 K. Because no guest solvent molecules are present in **1b**, the data could be plotted in Arrhenius fashion, as shown in Figure 4. The experimentally determined activation energy for the phenyl ring flip in **1b**, 43(6) kJ/mol, is larger than that expected for free TPE by approximately 20 kJ/mol. This suggests that indeed, the torsion of the phenyl ring in **1b** is impeded relative to solution-phase TPE, and is likely the cause of fluorescence turn-on in the TPE-based MOF. The pre-exponential factor, which can be interpreted as the barrier-less flipping rate of the pure phe-nylene bridge,[28,29] is 2.2×10^{11} Hz and is somewhat smaller than those of phenylene bridges in related porous materials such as MOF-5[30,31] and periodically-ordered mesoporous organosili-ca.[22] It is conceivable, however, that intramolecular steric effects converge to decrease the pre-exponential factor in TPE derivatives relative to phenylene itself.

One essential aspect of the NMR data interpretation relates to the stability and identity of the sample during the heating cycle. As for **1H**, heating of **1a** above 150 °C causes loss of both bound and unbound DEF molecules and is accompanied by significant structural changes and formation of a new phase, **1c**. In **1c**, fused 2D sheets bring phenyl rings on adjacent TPE cores in close proximity, giving rise to short Ph···Ph contacts of ~ 5 Å (measured between the centroids of the phenyl rings), in line with those observed in molecular crystals of TPE derivatives and solid TPE itself.[32]

Expectedly, just like TPE, **1c** exhibits Pake patterns at both low and high temperature, reinforcing the observation that close-packed TPE cores prohibit torsional motion of their phe-nyl(ene) components. Importantly, however, if **1b** is heated below 150 °C (i.e. the temperature range of our NMR experiments) its structure and the large Ph···Ph separation conducive to fast phenyl ring flipping, is maintained. This important fact was verified by both single crystal and powder X-ray analysis. Thus, single crystal X-ray diffraction of **1b** at 100 °C showed that no significant structural changes occur relative to **1a**. Although single crystals of **1b** do not survive heating at 150 °C, powder X-ray analysis of the sample used for the NMR experiments showed a pattern that matched that of **1b**, with only small peaks corresponding to the completely desolvated phase, **1c** (see Figure 2 and below). Because phenyl ring motion in **1c** is in the slow-exchange regime in this temperature range, its presence does not affect the dynamic line shapes used for the Arrhenius plot for **1b**, and are a minor contributor only to the Pake singularities with large quadrupolar splitting. In addition, ^{13}C CP-MAS NMR spectra of **1c** and of fully desolvated **1H** illustrate that both of these compounds exhibit similar resolution and line shape, which is consistent with a rigid

lattice with motion that is slower than what is detectable with this technique (< 10^2 Hz) (Figure 5). This finding agrees with the ^{2}H NMR results, which show that the ring motions are in the slow exchange regime.

To understand the origin of the activation barrier in **1b**, especially in comparison to TPE itself, the ring flipping process in both **1b** and TPE was probed by DFT calculations. The calculated values of the activation barriers for ring flipping in a truncated model of **1b** and gas-phase TPE are 49 kJ/mol and 24 kJ/mol, respectively. Clearly, despite the axial symmetry of phenylene rings in H_4TCPE, which should allow fast flipping in a sterically unhindered environment such as the pores of **1b**, phenyl ring flipping in **1b** is much more sluggish than in TPE itself. To understand the origin of the increased barrier in **1b** and the differences between the PESs of **1b** and TPE, a more detailed look at the steric and electronic contributions to these was performed. The electronic contribution was probed by considering ring flipping in styrene and benzoic acid, as well as vinylbenzoic acid (Figures S6 and S8). These molecules have similar electronic structures to the benzoate units in the truncated model of **1b**, but their phenyl groups lack vicinal phenyl rings that could sterically hinder rotation. The barrier to phenyl ring flipping in these can therefore be assumed to be completely electronic in origin. The electronic component of the PES for ring flipping in TPE could therefore be reconstructed from the PES of styrene, even though the energy contributions were not necessarily expected to be additive. This implied that the barrier for ring flipping in gas-phase TPE is almost completely electronic in origin, and the steric interactions expected to occur at a C_{Ar}–C_{Ar}–C=C dihedral angle of 0° are avoided due to a number of small geometrical distortions that correspond to low energy vibrational modes (Table 1). Rationalizing the shape of the PES of **1b** is more complicated because it cannot be reconstructed by simply summing the contributions from the PESs of styrene and benzoic acid. Because in **1b** itself the ethylene core is perpendicular to the carboxylate groups, the effect of the electronic contribution to the overall barrier for ring flipping is expected to be rather insignificant (Figure S8). To attest this, an atoms-in-molecules analysis of the C–C single bonds at select points on the PES was performed (Table S7).[33]

Since the density at the critical point is indicative of the bond order, the sum of the electron densities at each of the C–C single bond critical points should be indicative of the amount of electron delocalization throughout the molecule, and, by extension, the stability of the conformation at each point. Figure 7 illustrates how the sum of the densities at the C–C critical points mirrors the shape of PES. A key point is that the lowest total density, which should correspond to the least stable conformation is found at a local maximum. This indicates that the global maximum found at 5° (49 kJ/mol) is not entirely electronic in origin and must have a considerable steric contribution. Investigation of the geometry at the maximum in the PES of **1** (Figure 6) shows that the ortho-hydrogen atom on one phenyl ring is directed into the **π**-cloud of the vicinal *cis*-phenyl ring. Unlike in gas-phase TPE, where low energy geometric distortions to the TPE core allow the steric maximum to be avoided (Figure 6), the TPE core in **1b** is *drawn tight*, thereby forcing the phenyl rings to remain in close proximity during the ring flipping process.

This computational analysis highlights the following points:

1. Low-energy vibrational modes in the TPE core minimize inter-ring steric interactions and allow ring flipping to occur with a low barrier (25 kJ/mol).
2. The drawing of the TPE core by the framework forces these steric interactions to occur, leading to a significantly higher barrier for ring flipping (49 kJ/mol) that is in good agreement with the experimentally derived barrier.

The relative importance of the C=C bond twist and phenyl ring torsion in quenching the fluorescence in molecular TPE derivatives has been addressed before and it was concluded that the latter has higher contribution to the non-radiative decay of the excited state.[34] Our results are in line with this observation and allow us to establish a connection between the two: diminution of the C=C twist angle by drawing of the TPE core in **1b** causes a larger steric barrier for phenyl torsion/flipping, suggesting that a relatively large C=C twist angle or a flexible core is required for a low-barrier phenyl ring torsion. The activation barrier for ring flipping in **1b** is comparable to the activation energies for phenylene-linked porous materials.[22,29,30,36] For instance, activation energies for 1,4-aromatic dicarboxylate-based MOFs range from 21–53 kJ/mol (Table 2). Although some of these are higher than the activation energy for ring flipping in **1b**, the differences can be entirely attributed to conjugation-stabilized conformations in which the carboxylate groups and the phenylene ring are coplanar. We confirmed computationally that the PES constructed for ring-flipping in terephthalic acid gives an activation energy of 50 kJ/mol when both carboxylate groups are held coplanar, in good agreement with experimentally observed activation energies for MOFs constructed from this ligand. In the absence of conjugating groups, exemplified by the pyra-zine-bridged structures, a much lower activation energy is found. In these, because pyrazine is primarily a sigma-donating ligand, there is little energetic cost for ring flipping, which must only overcome a weak 3-type interaction with the d^{10} metal ion. Importantly, because the origin of the activation barrier in **1b** is enforced partly by coordination in a rigid lattice and is therefore not inherently borne in the ligand, strategies can be envisioned for reducing the activation barrier for ring-flipping. These strategies include:

1. Designing MOFs where *AIE-type chromophores are well separated spatially*. This is necessary to avoid aggregation in the empty material, and to ensure porosity for analyte adsorption.
2. Maintaining the *flexibility in the TPE core* to ensure that low-energy vibrational modes are not eliminated in the empty material. This could be implemented, for instance, by leaving two *dangling/unsubstituted phenyl rings* which should maintain dynamics in the fast flipping regime.
3. *Minimizing ligand conjugation* to reduce the contribution of an electronic component to the ring-flipping barrier. This could be achieved for instance by enforcing a perpendicular orientation between the ethylene core and the metal-binding functional groups, as in **1**, by using acetylene spacers to ‘insulate’ the phenyl ring from orientation-inducing conjugation, or by using non-conjugating ligating groups.

The criteria outlined above would allow the design of true turn-on MOF sensors. In such sensors, AIE-type chromo-phores with low-barrier ring flipping would completely quench the fluorescence in the empty porous materials. Fluorescence would then only be turned-on in the presence of analyte guests that can hinder the rotation of the phenylene ring, thereby eliminating the low-energy non-radiative excited state quenching pathways. MOFs are ideal candidates for incorporating such strategies because they lend themselves to modular synthetic design.[43,48–56] We envision that these strategies are not limited to TPE-based ligands and should be more broadly applicable to the construction of switchable luminescent MOFs from a wide variety of AIE-type ligands.

Experimental section

Materials

$Zn(NO_3)_2 \cdot 6H_2O$ (98%, Strem Chemicals), Br_2 (≥ 99.5%, Sigma-Aldrich), CuCN (99%, Strem Chemicals), Zn (dust, 98.6%, Mallinckrodt), oxalyl chloride (98%, Alfa Ae-sar),

$TiCl_4$ (≥ 99%, Sigma-Aldrich), $MgSO_4$ (98%, VWR), $AlCl_3$ (≥99%, Sigma-Aldrich), *N,N′*-dimethylethylenediamine (99%, Sigma-Aldrich), dichloromethane (HPLC grade, Honeywell), methanol (99.9%, VWR), DEF (> 95%, TCI Ameri-ca), *N,N*-diethylformamide (99.8%, VWR), ethanol (ACS grade, Mallinckrodt), ethylene glycol (AR grade, Mallinckrodt), ethyl acetate (VWR), tetrahydrofuran (ACS grade, Mallinckrodt), toluene (Sigma-Aldrich, ACS), C_6D_6 (Cambridge Isotopes), $CDCl_3$ (Cambridge Isotopes), CD_3OD (Cambridge Isotopes), and DMSO-d_6 (Cambridge Isotopes) were used as received.

Tetraphenylethylene-d_{20}

($C_{26}D_{20}$, TPE-d_{20}). The synthetic sequence for the preparation of this material is shown in Scheme 1. Benzophenone-d_{10} was synthesized from benzened_6 based on a known procedure,[57] and was then heated (5.47 g, 0.03 mmol) to reflux in the presence of $TiCl_4$ (8.60 g, 0.05 mmol) and Zn dust (5.90 g, 0.09 mol) under McMurry conditions[23] to give 4.60 g (0.01 mol) of perdeutero-tetraphenylethylene (87% yield). ^{2}H NMR ($CHCl_3$): δ = 7.05 (br) ppm; ^{H} NMR ($CDCl_3$, 500 MHz): δ = 126.20 (t), 127.24 (t), 131.00 (t), 140.93 (s), 143.68 (s) ppm. IR (neat, cm^{-1}): 2281 (s), 2269 (s), 1617 (w), 1563 (m), 1385 (w), 1322 (s), 1279 (w), 1202 (w), 959 (w), 878 (w), 855 (s), 841 (m), 822 (vs), 788 (w), 763 (w). Elemental analysis calculated for $C_{26}D_{20}$: C, 88.57; H(D), 6.07. Found: C, 88.67; H(D), 5.87.

Tetrakis(4-cyanophenyl)ethylene-d_{16}

($C_{30}D_{16}N_4$, H_4TCNPE-d_{16}). H_4TCNPE-d_{16} was prepared from TPE-d_{20} following a recently published synthetic route for the protonated analogue.[21] ^{13}C NMR (CD_2Cl_2, 500 MHz) δ = 111.78 (s), 118.56 (s), 131.56 (t), 132.14 (t), 141.75 (s), 145.82 (s) ppm. IR (neat, cm^{-1}): 2294 (w), 2225 (vs), 1573 (s), 1414 (w), 1321 (m), 1291 (w), 1109 (m), 869 (w), 827 (m), 759 (w), 743 (w), 718 (w), 677 (w). Elemental analysis for calculated for $C_{30}D_{16}N_4$: C, 80.36; H(D), 3.72; N, 12.49. Found: C, 80.10; H(D) 3.75; N, 12.30.

Tetrakis(4-carboxyphenyl)ethylene-d_{16}

($C_{30}H_4D_{16}O_8$, H_4TCPE-d_{16}). H_4TCPE-d_{16} was synthesized by hydrolysis of the corresponding nitrile following the published procedure for the protonated analogue.[21] ^{2}H NMR (CH_3OH, 500 MHz): δ = 7.19 (br), 7.86 (br) ppm; ^{13}C NMR ($CDCl_3$, 500 MHz): δ = 128.8 (m), 129.29 (s), 130.49 (m), 141.10 (s), 146.32 (s), 166.96 (s) ppm. IR (neat, cm^{-1}): 2972 (w, b), 2225 (w), 1687 (vs), 1578 (s), 1542 (w), 1439 (m), 1376 (w), 1327 (w), 1259 (b, s), 1206 (s), 1078 (w), 871 (w), 841 (w), 816 (w), 786 (w), 746 (w), 691 (w). Elemental analysis calculated for $C_{30}H_4D_{16}O_8 \cdot H_2O$: C, 66.4; H(D), 4.21. Found: C, 66.09; H(D), 3.93.

Synthesis of Zn_2(TCPE-d_{16})$(DEF)_2 \cdot 2$DEF (1a)

This compound was synthesized in an identical procedure as **1H**. IR (neat, cm^{-1}): 2979 (w), 2939 (w), 2878 (w), 2272 (w), 1634 (vs), 1578 (m), 1559 (m), 1442 (s), 1382 (vs), 1309 (w), 1265 (w), 1215 (w), 1106 (w), 881 (w), 832 (w), 820 (w), 703 (w), 677 (w). Elemental analysis calculated for **1a**·H_2O: C, 55.92; H(D), 5.91; N, 5.22. Found C 55.74, H 5.73, N 5.10.

X-ray crystal structure determination

Diffraction-quality single crystals of **1a, 1b,** and **TPE**-d_{20} were mounted using mineral oil and epoxy on Kapton loops. Diffraction data (ϕ- and ω-scans) at 100 K, 298 K, and 373 K were collected on a Bruker-AXS X8 Kappa Duo diffractometer coupled to a Smart APEX II CCD detector with MoKα radiation (λ = 0.71073 Å) from an IμS-micro source. Absorption and polarization corrections were applied using SADABS.[58] The structure was solved by direct methods using SHELXS and refined against F^2 on all data by full-matrix least squares

with SHELXL-97.[59] All non-hydrogen atoms were refined anisotropically and were included in the model at geometrically calculated positions. The crystallographic data for TPE-d_{20} and **1** are shown in Table S1.

^{2}H NMR Spectroscopy

Experiments were conducted on a home-built spectrometer (courtesy of Dr. Dave Ruben) operating at 61 MHz for ^{2}H using a single-channel transmission line probe with 3.2 mm coil. Spectra were obtained using a quad-rupolar echo sequence[60] with an 8-step phase cycling[61] using a $\pi/2$ pulse of 2.0 μs and a delay of 30 μs between the two pulses. Phenyl ring motional dynamics were determined by simulations of the experimental ^{2}H powder lineshapes using TURBOPOWDER.[62]

^{13}C MAS NMR Spectroscopy

Experiments were performed at 16.4 T (697.8 MHz, ^{1}H) using a home-built spectrometer (courtesy of Dr. Dave Ruben) and a 3.2 mm Che-magnetics triple-channel magic-angle spinning probe. Samples were ground using a mortar and pestle and packed in 3.2 mm ZrO_2 rotors (~28 μl sample volume). Spectra were acquired at spinning frequencies of 10 kHz, with 512–4096 co-added transients and recycle delays between 3 and 120 seconds, using either a Bloch decay or Cross-Polarization[63] (υ_{rf} of 83 kHz for ^{1}H and ^{13}C, τ_{CP} = 2.0 ms) and two pulse phase modulation (TPPM) proton decoupling[64] for naturally abundant ^{13}C deu-terated and protonated samples. ^{13}C experiments were referenced to adamantane at 38.48 ppm relative to TMS.[65]

Computational Details

Calculations were performed using the ORCA 2.8 quantum chemistry program package from the development team at the University of Bonn.[66] In all cases the LDA and GGA functionals employed were those of Perdew and Wang (PW-LDA, PW91).[67] Calculations were performed using the TZV basis set for hydrogen, the TZV(p) basis set for main group atoms and TZV(2pf) for zinc.[68] Spin-restricted Kohn–Sham determinants have been chosen to describe the closed-shell wavefunctions, employing the RI approximation and the tight SCF convergence criteria provided by ORCA. Numerical frequency calculations were performed on the optimized structures when size would permit. The atoms in molecules analysis was performed using Xaim.[69]

Other physical measurements

Thermogravimetric analysis (TGA) was performed on a TA Instruments Q500 Thermo-gravimetric Analyzer at a heating rate of 0.5 °C/min under a nitrogen gas flow of 90 mL/min. Infrared spectra were obtained on a PerkinElmer Spectrum 400 FT-IR/FT-FIR Spectrometer equipped with a Pike Technologies GladiATR attenuated total reflectance accessory. Solution NMR spectra were collected on a Varian 300 or a Varian Inova-500 NMR spectrometer. ^{2}H spectra were referenced to the natural abundance ^{2}H peak in protonated solvents; ^{13}C and ^{1}H spectra were referenced to natural abundance ^{13}C peaks and residual ^{1}H peaks of deuterated solvents, respectively. Powder X-ray diffraction patterns for **1a** and **1b** were recorded on a Bruker Advance D8 diffractometer using Nickel-filtered Cu-Kα radiation (λ = 1.5418 Å), with accelerating voltage and current of 40 kV and 40 mA, respectively. A PXRD pattern for **1c** was collected at station 11-B at the Argonne National Laboratory using synchrotron radiation (λ = 0.413073 Å). Samples for PXRD were prepared by placing a thin layer of the appropriate material on a silicon (510) crystal plate for **1a** and **1b**, and by sealing **1c** in a Kapton capillary.

Supplementary Material

Refer to Web version on PubMed Central for supplementary material.

Acknowledgments

This work was supported as part of the Center for Excitonics, an Energy Frontier Research Center funded by the U.S. Department of Energy, Office of Science, Office of Basic Energy Sciences under Award Number DE-SC0001088 (MIT). We would like to thank the 11 B-sector team at the Advanced Photon Source, Argonne National Laboratory, which was supported by the U. S. Department of Energy, Office of Science, Office of Basic Energy Sciences, under Contract No. DE-AC02–06CH11357. Grants from the NSF also provided instrument support to the DCIF and single crystal X-ray diffraction facility at MIT (CHE-9808061, DBI-9729592, CHE-0946721). R.G.G. is supported through the National Institute of Health (NIH grants EB001960 and EB002026). V.K.M. thanks the Natural Sciences and Engineering Research Council of Canada for a postdoctoral fellowship. We thank Tarun Narayan for writing the Matlab routine for modeling the structure of **1c**, and Minyuan Li for assistance with the production of the TOC graphic.

References

1. Lakowicz, JR. Principles of fluorescence spectroscopy. 2. Kluwer Academic/Plenum; New York: 1999.
2. Birks, JB. Photophysics of aromatic molecules. Wiley-Interscience; London, New York: 1970.
3. Tang CW, Vanslyke SA. Appl Phys Lett. 1987; 51:913–915.
4. Zhao Z, Chen S, Deng C, Lam JWY, Chan CYK, Lu P, Wang Z, Hu B, Chen X, Kwok HS, Ma Y, Qiu H, Tang BZ. J Mater Chem. 2011; 21:10949–10956.
5. Hong Y, Lam JWY, Tang BZ. Chem Soc Rev. 2011; 40:5361–5388. [PubMed: 21799992]
6. Yuan WZ, Lu P, Chen S, Lam JWY, Wang Z, Liu Y, Kwok HS, Ma Y, Tang BZ. Adv Mater. 2010; 22:2159–2163. [PubMed: 20564253]
7. Chen JW, Law CCW, Lam JWY, Dong YP, Lo SMF, Williams ID, Zhu DB, Tang BZ. Chem Mater. 2003; 15:1535–1546.
8. Mei J, Wang J, Sun JZ, Zhao H, Yuan WZ, Deng CM, Chen SM, Sung HHY, Lu P, Qin AJ, Kwok HS, Ma YG, Williams ID, Tang BZ. Chem Sci. 2012; 3:549–558.
9. Gao BR, Wang HY, Yang ZY, Wang H, Wang L, Jiang Y, Hao YW, Chen QD, Li YP, Ma YG, Sun HB. J Phys Chem C. 2011; 115:16150–16154.
10. Tong H, Hong Y, Dong Y, Häussler M, Lam JWY, Li Z, Guo Z, Guo Z, Tang BZ. Chem Commun. 2006:3705–3707.
11. Tong H, Hong Y, Dong Y, Häussler M, Li Z, Lam JWY, Dong Y, Sung HHY, Williams ID, Tang BZ. J Phys Chem B. 2007; 111:11817–11823. [PubMed: 17877385]
12. Liu Y, Tang Y, Barashkov NN, Irgibaeva IS, Lam JWY, Hu R, Birimzhanova D, Yu Y, Tang BZ. J Am Chem Soc. 2010; 132:13951–13953. [PubMed: 20853831]
13. Hong Y, Meng L, Chen S, Leung CWT, Da LT, Faisal M, Silva DA, Liu J, Lam JWY, Huang X, Tang BZ. J Am Chem Soc. 2012; 134:1680–1689. [PubMed: 22191699]
14. Liu Y, Deng C, Tang L, Qin A, Hu R, Sun JZ, Tang BZ. J Am Chem Soc. 2011; 133:660–663. [PubMed: 21171593]
15. Yuan WZ, Chen S, Lam JWY, Deng C, Lu P, Sung HHY, Williams ID, Kwok HS, Zhang Y, Tang BZ. Chem Commun. 2011; 47:11216–11218.
16. Qin A, Lam JWY, Tang BZ. Prog Polym Sci. 2012; 37:182–209.
17. Liu J, Zhong Y, Lam JWY, Lu P, Hong Y, Yu Y, Yue Y, Faisal M, Sung HHY, Williams ID, Wong KS, Tang BZ. Macromolecules. 2010; 43:4921–4936.
18. Tseng NW, Liu J, Ng JCY, Lam JWY, Sung HHY, Williams ID, Tang BZ. Chem Sci. 2012; 3:493–497.
19. Hong Y, Lam JWY, Tang BZ. Chem Commun. 2009:4332–4353.
20. Qin A, Tang L, Lam JWY, Jim CKW, Yu Y, Zhao H, Sun J, Tang BZ. Adv Funct Mater. 2009; 19:1891–1900.

21. Shustova NB, McCarthy BD, Dincã M. J Am Chem Soc. 2011; 133:20126–20129. [PubMed: 22074054]
22. Vogelsberg CS, Bracco S, Beretta M, Comotti A, Sozzani P, Garcia-Garibay MA. J Phys Chem B. 2012; 116:1623–1632. [PubMed: 22220838]
23. Mukaiyama T, Sato T, Hanna J. Chem Lett. 1973:1041–1044.
24. Rice DM, Wittebort RJ, Griffin RG, Meirovitch E, Stimson ER, Meinwald YC, Freed JH, Scheraga HA. J Am Chem Soc. 1981; 103:7707–7710.
25. Rice DM, Meinwald YC, Scheraga HA, Griffin RG. J Am Chem Soc. 1987; 109:1636–1640.
26. Cholli AL, Dumais JJ, Engel AK, Jelinski LW. Macromolecules. 1984; 17:2399–2404.
27. Kolodziejski W, Klinowski J. Chem Rev. 2002; 102:613–628. [PubMed: 11890752]
28. Laidler, KJ. Reaction kinetics. Pergamon Press; Oxford, New York: 1963.
29. Weston, RE.; Schwarz, H. Chemical kinetics. Prentice-Hall; Englewood Cliffs, N. J: 1972.
30. Gould SL, Tranchemontagne D, Yaghi OM, Garcia-Garibay MA. J Am Chem Soc. 2008; 130:3246–3247. [PubMed: 18288839]
31. Horike S, Shimomura S, Kitagawa S. Nature Chem. 2009; 1:695–704. [PubMed: 21124356]
32. Hoekstra A, Vos A. Acta Crystallogr, Sect B:-Struct Sci. 1975; 31:1716–1721.
33. Bader, RFW. Atoms in molecules: a quantum theory. Clarendon Press; Oxford University Press; Oxford New York: 1990.
34. Shultz DA, Fox MA. J Am Chem Soc. 1989; 111:6311–6320.
35. Li H, Eddaoudi M, O'Keeffe M, Yaghi OM. Nature. 1999; 402:276–279. ST - Design and synthesis of an exception.
36. Kolokolov DI, Stepanov AG, Guillerm V, Serre C, Frick B, Jobic H. J Phys Chem C. 116:12131–12136.
37. Meilikhov M, Yusenko K, Torrisi A, Jee B, Mellot-Draznieks C, Poeppl A, Fischer RA. Angew Chem Int Ed. 2010; 49:6212–6215.
38. Kolokolov DI, Jobic H, Stepanov AG, Guillerm V, Devic T, Serre C, Ferey G. Angew Chem Int Ed. 2010; 49:4791–4794.
39. Serre C, Millange F, Thouvenot C, Nogues M, Marso-lier G, Louer D, Ferey G. J Am Chem Soc. 2002; 124:13519–13526. [PubMed: 12418906]
40. Eddaoudi M, Kim J, Rosi N, Vodak D, Wachter J, O'Keeffe M, Yaghi OM. Science. 2002; 295:469–472. [PubMed: 11799235]
41. Morris W, Taylor RE, Dybowski C, Yaghi OM, Garcia-Garibay MA. J Mol Struct. 2011; 1004:94–101.
42. Winston EB, Lowell PJ, Vacek J, Chocholousova J, Michl J, Price JC. Phys Chem Chem Phys. 2008; 10:5182–5188.
43. Rocha J, Carlos LD, Almeida Paz FA, Ananias D. Chem Soc Rev. 2011; 40:926–940. [PubMed: 21180775]
44. Rodriguez-Velamazan A, Gonzalez MA, Real JA, Castro M, Carmen Munoz M, Gaspar AB, Ohtani R, Ohba M, Yoneda K, Hijikata Y, Yanai N, Mizuno M, Ando H, Kitagawa S. J Am Chem Soc. 2012; 134:5083–5089. ST - A Switchable Molecular Rotator: Neu. [PubMed: 22364147]
45. Horike S, Matsuda R, Tanaka D, Matsubara S, Mizuno M, Endo K, Kitagawa S. Angew Chem Int Ed. 2006; 45:7226–7230.
46. Chun H, Dybtsev DN, Kim H, Kim K. Chem Eur J. 2005; 11:3521–3529. [PubMed: 15761853]
47. Comotti A, Bracco S, Valsesia P, Beretta M, Sozzani P. Angew Chem Int Ed. 2010; 49:1760–1764.
48. Allendorf MD, Bauer CA, Bhakta RK, Houk RJT. Chem Soc Rev. 2009; 38:1330–1352. [PubMed: 19384441]
49. Bauer CA, Timofeeva TV, Settersten TB, Patterson BD, Liu VH, Simmons BA, Allendorf MD. J Am Chem Soc. 2007; 129:7136–7144. [PubMed: 17503820]
50. Lee CY, Farha OK, Hong BJ, Sarjeant AA, Ngu-yen ST, Hupp JT. J Am Chem Soc. 2011; 133:15858–15861. [PubMed: 21916479]
51. Lu G, Hupp JT. J Am Chem Soc. 2010; 132:7832–7833. [PubMed: 20486704]

52. Wang C, Lin W. J Am Chem Soc. 2011; 133:4232–4235. [PubMed: 21384886]
53. Kent CA, Liu D, Ma L, Papanikolas JM, Meyer TJ, Lin W. J Am Chem Soc. 2011; 133:12940–12943. [PubMed: 21776996]
54. Rieter WJ, Taylor KML, Lin W. J Am Chem Soc. 2007; 129:9852–9853. [PubMed: 17645339]
55. Stylianou KC, Heck R, Chong SY, Bacsa J, Jones JTA, Khimyak YZ, Bradshaw D, Rosseinsky MJ. J Am Chem Soc. 2010; 132:4119–4130. [PubMed: 20201518]
56. Chen B, Wang L, Zapata F, Qian G, Lobkovsky EB. J Am Chem Soc. 2008; 130:6718–6719. [PubMed: 18452294]
57. Edelmann FT. Inorg Chim Acta. 2004; 357:4592–4595.
58. Sheldrick, GM. SADABS - A program for area detector absorption corrections. 2004.
59. Sheldrick GM. Acta Crystallogr, Sect A. 2008; 64:112–122. [PubMed: 18156677]
60. Davis JH, Jeffrey KR, Bloom M, Valic MI, Higgs TP. Chem Phys Lett. 1976; 42:390–394.
61. Griffin RG. Methods Enzymol. 1981; 72:108–174. [PubMed: 7311829]
62. Wittebort RJ, Olejniczak ET, Griffin RG. J Chem Phys. 1987; 86:5411–5420.
63. Pines A, Waugh JS, Gibby MG. J Chem Phys. 1972; 56:1776–1777.
64. Bennett AE, Rienstra CM, Auger M, Lakshmi KV, Griffin RG. J Chem Phys. 1995; 103:6951–6958.
65. Morcombe CR, Zilm KW. J Mag Reson. 2003; 162:479–486.
66. Neese, F. ORCA–an ab initio, Density Functional and Sem-iempirical program package, version 2.8.0. 2009.
67. Perdew J, Wang Y. Phys Rev B. 1992; 46:12947–12954.
68. Schafer A, Horn H, Ahlrichs R. J Chem Phys. 1992; 97:2571–2577.
69. Ortiz, JC.; Bo, C. Tarra-gona. Spain: Xaim-Universitat Rovira i Virgili. http://www.quimica.urv.es/XAIM/

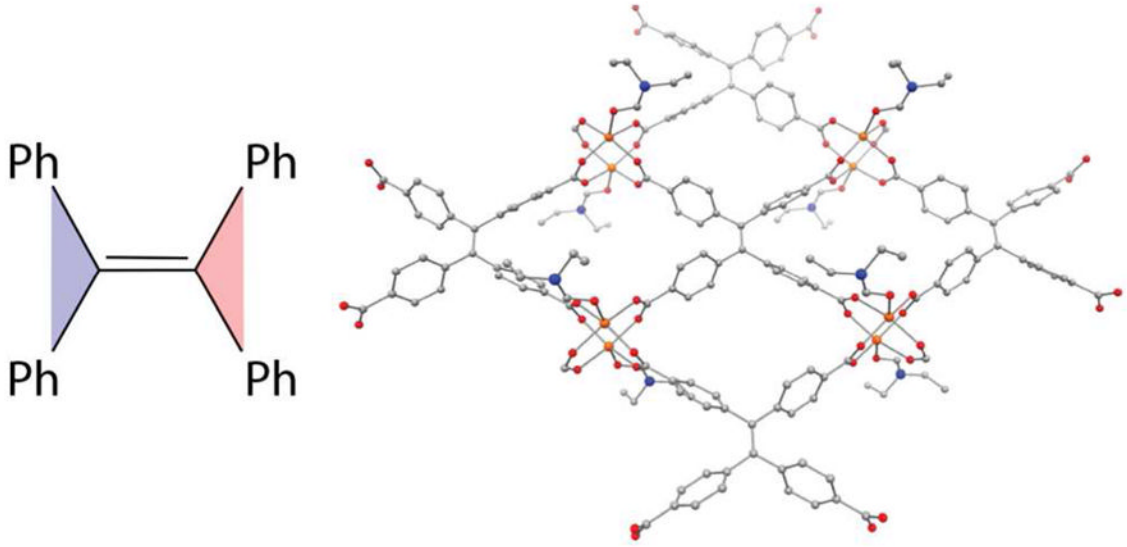

Figure 1.

The planes used to define the twist in the ethylene core (left), and a portion of the X-ray crystal structure of Zn_2(TCPE) that is representative of both **1H** and **1** (right). Orange, red, blue, and grey spheres represent Zn, O, N, and C atoms, respectively. H/D atoms were removed for clarity.

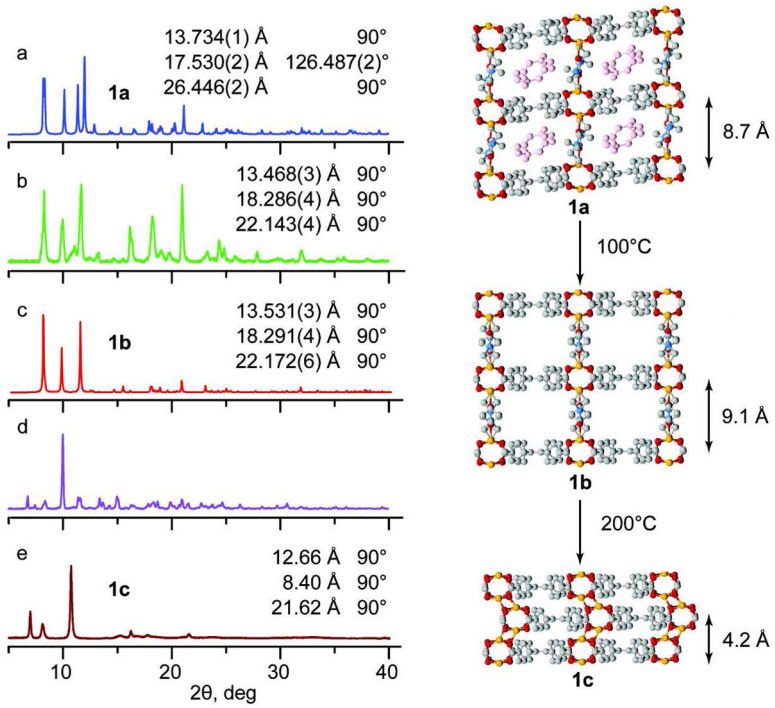

Figure 2.

Temperature-dependent X-ray diffraction studies of **1**. Left column: PXRD patterns of (a) **1a** calculated from the X-ray crystal structure determined at 100 K, (b) **1a** collected at room temperature, (c) **1b** calculated from X-ray structure at 373 K, (d) the sample used in the ^{2}H NMR study, and (e) **1c**. Right column: X-ray crystal structures of **1a** collected at 100 K, **1b** collected at 373 K, and the simulated structure of **1c** based on the PXRD data. Golden, red, blue, and grey spheres represent Zn, O, N, and C atoms, respectively. Guest DEF molecules are shown in pink. H/D atoms have been removed for clarity.

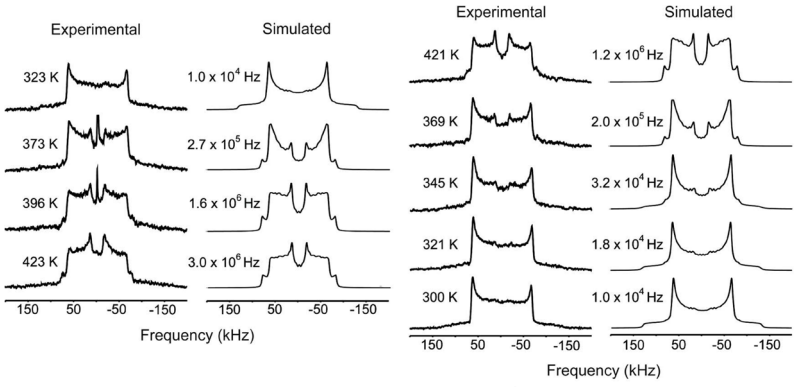

Figure 3.

Experimental and simulated quadrupolar spin-echo solid-state ^{2}H NMR spectra of **1a** during heating and transformation into **1b** (left), and of **1b** during cooling (right).

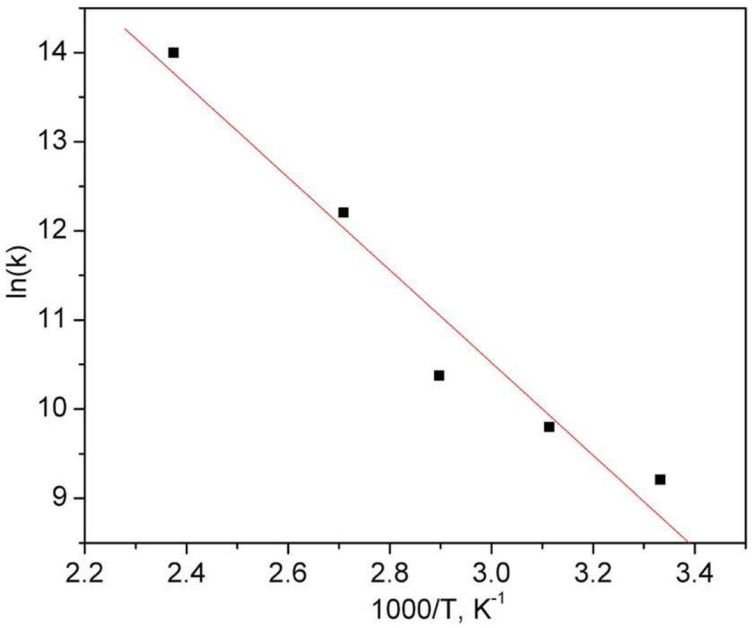

Figure 4.
Arrhenius plot of the two-fold phenyl exchange rate in **1b** during cooling.

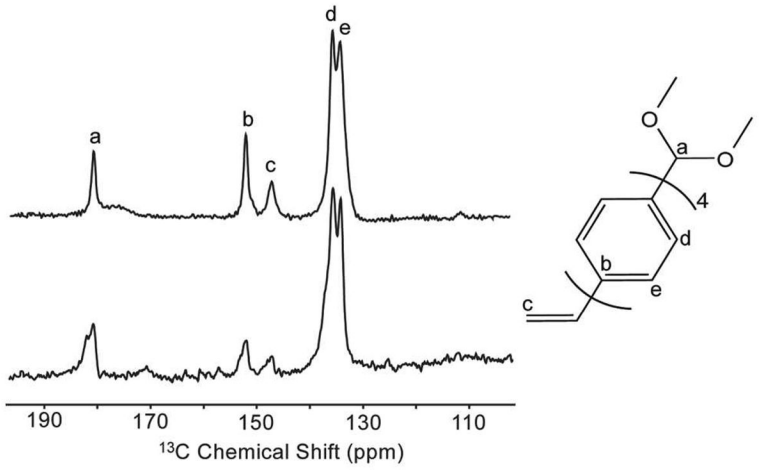

Figure 5.
^{13}C CP-MAS NMR spectra of fully desolvated **1H** (top) and **1c** (bottom).

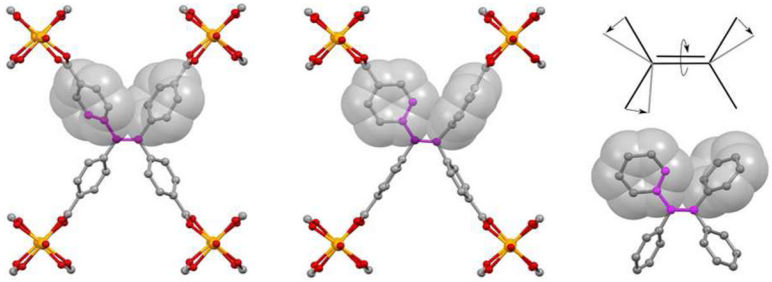

Figure 6.
DFT-calculated structures of truncated formate-capped models of **1b** with a fixed orientation of one phenyl ring at 125° (left) and 5° (middle), and of TPE with a fixed orientation of the phenyl ring at 0° (right). The scheme illustrates the distortion in the TPE core that occurs to minimize the steric repulsion, namely in-plane bends of the C_{Ar}-C=C angles and the C=C twist. The models are depicted without hydrogen atoms for clarity. Yellow, red, and grey spheres represent Zn, O, and C atoms, respectively. The carbon atoms that define the dihedral angles used to model the PESs are shown in purple.

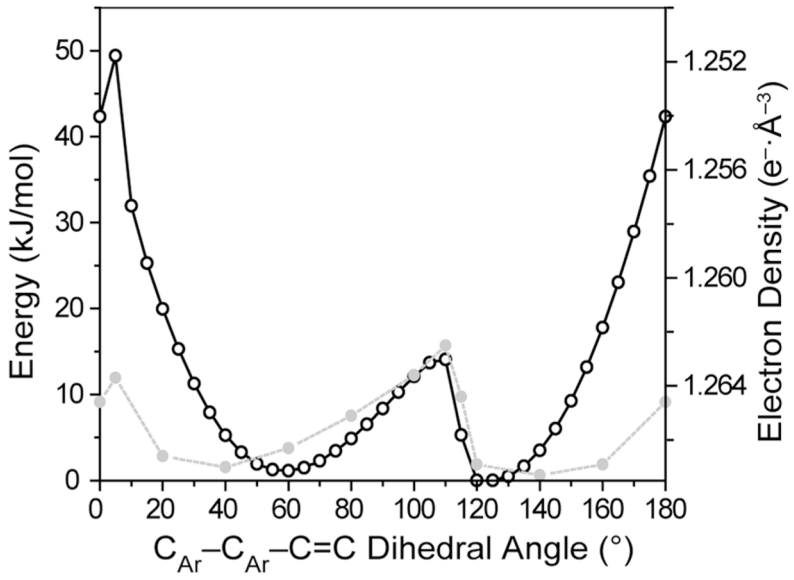

Figure 7.

The PES for the flipping of one phenyl ring in a truncated model of **1b** (○) and sum of the electron density at the C–C single bond critical points (●). The electron density axis has been reversed and scaled for clarity. Lines have been added as a visual guide.

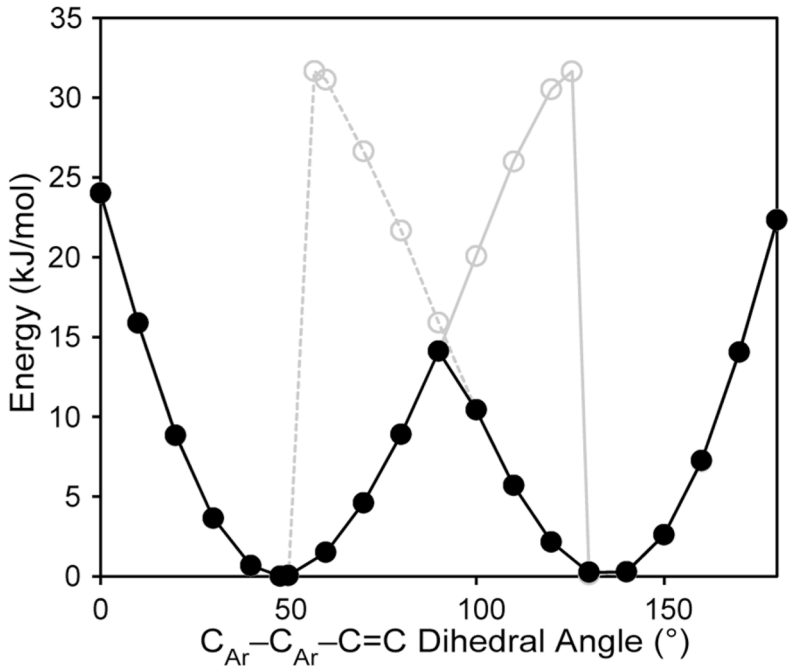

Figure 8.
The PES for the flipping of one phenyl ring in a model of TPE. The solid line with black circles indicates the lowest energy surface constructed from the forward (solid gray line and hollow circles) and the reverse (hashed gray line) direction ring-flip PESs.

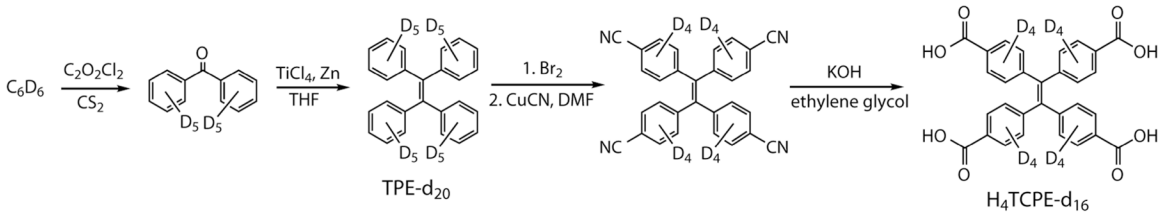

Scheme 1.
Synthesis of H_4TCPE-d_{16}.

Table 1

DFT-calculated low-energy vibrational modes for TPE.

Energy (cm^{-1})		Vibrational Mode
6	ν_1	C–C=C–C torsion
29	ν_2	C_{Ar}–C_{Ar}–C=C torsion
39	ν_3	C_{Ar}–C_{Ar}–C=C torsion
54	ν_4	Aryl rocking
58	ν_5	C_{Ar}–C_{Ar}–C=C torsion
65	ν_6	Aryl rocking
69	ν_7	C_{Ar}–C_{Ar}–C=C torsion
72	ν_8	C_{Ar}–C_{Ar}–C=C torsion
78	ν_9	C_{Ar}–C_{Ar}–C=C torsion

Table 2

Activation energies and discrete flipping models for known, structurally-rigid porous materials

Compound[a]	Flipping fragment	Bonds affected (torsion angle)[b]	Ea, kJ/mol	k_0c, s^{-1}	Model
$Zn_4O(BDC)_3$[30,35] (**MOF-5**)		2 × C_{Ar}–C_{COOH} (0°)	47±8	2.4×10^{12}	2 site jumps
VO(BDC)[36,37] (**MIL-47(V)**)		2 × C_{Ar}–C_{COOH} (0°)	45	0.88×10^{11}	2 site jumps
$Cr(OH)(BDC)(BDC)_x(H_2O)_y$[38,39] (**MIL-53(Cr)**)		2 × C_{Ar}–C_{COOH} (0°)	41	1.26×10^{11}	2 site jumps
$Zn_4O(BDC\text{-}NH_2)_3$[40,41](**IRMOF-3**)	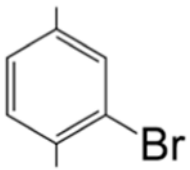	2 × C_{Ar}–C_{COOH} (0°)	21±8	1.3×10^{7}	2 site jumps
Zn4O(BDC-Br)$_3$[42,43] (**IRMOF-2**)	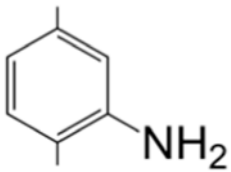	2 × C_{Ar}–C_{COOH} (0°)	31	–	–

Compound[a]	Flipping fragment	Bonds affected (torsion angle)[b]	Ea, kJ/mol	k_0c, s^{-1}	Model
$Fe(Pz)[Pt(CN)_4]$[44]	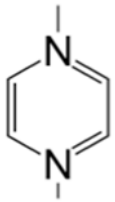	2 × $M–N_{pz}$	30(2)	3.0×10^{12}	4 site jumps
$CdNa(STP)(Pz)_{0.5}(H_2O)$[45]	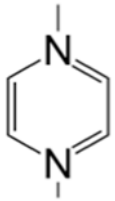	2 × $M–N_{pz}$	7.5	2.4×10^{6}	4 site jumps
$Zn_2(NDC)_2(dabco)$[45,46]	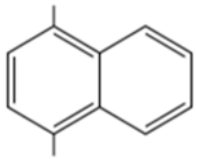	2 × $C_{Ar}–C_{COOH}$ (0°)	53	–	4 site jumps
Periodically Ordered Mesoporous Organosilica[22]		2 × $C_{Ar}–C_{C=C}$	38	1.7×10^{12}	2 site jumps
Periodically Ordered Mesoporous Organosilica[47]	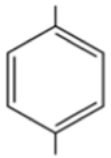	2 × $C_{Ar}–Si_{siloxane}$	55	–	2 site jumps

Compound[a]	Flipping fragment	Bonds affected (torsion angle)[b]	Ea, kJ/mol	k_0c, s^{-1}	Model
$Zr_6(OH)_4O_4(BDC)_6$[36] (**UiO-66(Zr)**)		2 × C_{Ar}–C_{COOH}	30±2	$0.5\pm0.8\times10^{12}$	2 site jumps

[a]BDC = 1,4-benzenedicarboxylate; BDC-NH_2 = 2-amino-1,4-benzenedicarboxylate; BDC-Br = 2-bromo-1,4-benzenedicarboxylate; Pz = pyrazine; STP = 2-sulfoterephthalate; NDC = 1,4-naphthalenedicarboxylate; dabco = 1,4-diazabicyclooctane.

[b]The torsion angle refers to the dihedral angle defined by the two para carboxylate groups.

[c]Pre-exponential factor in Arrhenius equation.